

Magnetized Plasma for Reconfigurable Subdiffraction Imaging

Shuang Zhang,^{1,*} Yi Xiong,¹ Guy Bartal,¹ Xiaobo Yin,^{1,2} and Xiang Zhang^{1,2,†}

¹*Nanoscale Science and Engineering Center, University of California, 5130 Etcheverry Hall, Berkeley, California 94720-1740, USA*

²*Materials Sciences Division, Lawrence Berkeley National Laboratory, 1 Cyclotron Road Berkeley, California 94720, USA*

(Received 10 March 2011; revised manuscript received 8 May 2011; published 13 June 2011)

We show that magnetized plasma with appropriately designed parameters supports nearly diffractionless propagation of electromagnetic waves along the direction of the applied magnetic field, arising from their unbounded equifrequency contour in the magnetized plasma. Such a unique feature can be utilized to construct subdiffraction imaging devices, which is confirmed by detailed numerical investigations. Subdiffraction imaging devices based on magnetic plasma do not require microfabrication normally entailed by construction of metamaterials; more importantly, they can be dynamically reconfigured by tuning the applied magnetic field or the plasma density, and therefore they represent a facile and powerful route for imaging applications.

DOI: 10.1103/PhysRevLett.106.243901

PACS numbers: 42.25.Bs, 52.25.Xz, 78.20.Ci

The progress in the field of metamaterials has shown many new striking physics [1,2] that may lead to many important applications, including subdiffraction imaging, slow light, and invisibility cloaking [3–6]. Imaging beyond the diffraction limit is of special importance because of many applications ranging from biological imaging in the optical regime to magnetic resonance imaging at radio frequencies. It has been shown that negative index metamaterial slabs were capable of magnifying the evanescent waves that carry the information of high spatial resolutions and recovering the fine features of the object at the image plane [2–4,7]. However, the spatial resolution of imaging using the negative index metamaterials is extremely sensitive to the presence of material loss and therefore limits their applications as practical superimaging devices.

Recently, it was shown that anisotropic media with mixed signs of permittivity tensor elements exhibit a very unique dispersion relation that supports hyperbolic equifrequency contour (EFC), allowing the propagation of electromagnetic waves with very large wave vectors [8–10]. As a result, superfine features of the objects can be transported by propagating waves through the medium. In comparison with the negative index slab, the imaging through a hyperbolic medium is highly robust against the presence of material loss; therefore, it represents a more practical approach for subdiffraction imaging. Artificial media with hyperbolic dispersion have been demonstrated recently in the form of metallic wire arrays, metal-dielectric multilayers, and Swiss roll magnetic resonators [11–14]. However, the fabrication of these media requires time-consuming microfabrication procedures, and the electromagnetic properties cannot be conveniently reconfigured in real time. Here we propose to employ magnetized plasma for achieving dynamically reconfigurable superimaging at the radio, microwave, and terahertz frequencies.

The electromagnetic properties of a lossless plasma are described by the Drude model $\varepsilon_p = 1 - \frac{\omega_p^2}{\omega^2}$, where

$\omega_p = \sqrt{Ne^2/\varepsilon_0 m}$ is the plasma frequency, N being the electron concentration. For electromagnetic waves with frequency below the plasma frequency, the plasma exhibits metalliclike properties and the waves cannot propagate through the plasma, whereas under a strong external dc magnetic field, the electromagnetic properties of the plasma are modified in such a way that they not only show direction-dependent wave propagation (anisotropy) but also exhibit optical activity for electromagnetic waves propagating along the direction of the magnetic field. In a magnetized plasma, the electrons circle around the direction of the magnetic field at the cyclotron frequency, given as $\omega_c = \frac{eB}{m}$. As a result, the permittivity takes the form of a tensor [15]:

$$\varepsilon = \begin{pmatrix} \varepsilon_1 & -i\varepsilon_2 & 0 \\ i\varepsilon_2 & \varepsilon_1 & 0 \\ 0 & 0 & \varepsilon_p \end{pmatrix}, \quad (1)$$

where $\varepsilon_1 = 1 + \frac{\omega_p^2}{\omega_c^2 - \omega^2}$, $\varepsilon_2 = \frac{\omega_p^2 \omega_c}{\omega(\omega_c^2 - \omega^2)}$, and $\varepsilon_p = 1 - \frac{\omega_p^2}{\omega^2}$. Notably, in the presence of an infinitely large applied magnetic field, the off-diagonal elements in Eq. (1) disappear, and the permittivity can be simply written as

$$\varepsilon = \begin{pmatrix} 1 & 0 & 0 \\ 0 & 1 & 0 \\ 0 & 0 & 1 - \frac{\omega_p^2}{\omega^2} \end{pmatrix}. \quad (2)$$

According to Eq. (2), a plasma under an infinitely strong magnetic field exhibits the same electromagnetic properties as an uniaxial anisotropic medium. Depending on whether the frequency of the electromagnetic wave is above or below the plasma frequency, the EFC of the magnetized plasma can be either elliptical or hyperbolic. In particular, for the electromagnetic frequency well below the plasma frequency, the hyperbolic EFC exhibits a very

flat feature, which lays the foundation for applications such as the hyperlens [11] and subwavelength endoscope [13].

However, in a realistic system, the magnitude of the magnetic field is always finite. Therefore, the off-diagonal elements in Eq. (1) still play an important role for determining the electromagnetic properties of the magnetized plasma. In the following, we will explore the potential of realistic magnetized plasma for subdiffraction imaging applications. The dispersion relation of magnetized plasma is given as [15]

$$\tan^2 \theta = -\frac{\varepsilon_p(n^2 - \varepsilon_R)(n^2 - \varepsilon_L)}{\varepsilon_1(n^2 - \varepsilon_X)(n^2 - \varepsilon_p)}, \quad (3)$$

where θ is the angle formed between the wave vector and the applied magnetic field, n is the refractive index, $\varepsilon_{L(R)} = 1 - \frac{\omega_p^2}{\omega(\omega \mp \omega_c)}$, and $\varepsilon_X = \frac{\varepsilon_R \varepsilon_L}{\varepsilon_1}$. The dispersion given by Eq. (3) shows very rich features depending on the relative values of ω , ω_p , and ω_c . Here we are interested only in the case where the electromagnetic frequency is far below the plasma frequency for the imaging purpose. We assume a realistic magnetized plasma system in which the plasma density is $1 \times 10^{12} \text{ cm}^{-3}$ (corresponding to $\omega_p = 5.64 \times 10^{10} \text{ rad/s}$) under an applied dc magnetic field ranging from 1 to 4 T, with the corresponding cyclotron frequency ranging from 1.76×10^{11} to $7.03 \times 10^{11} \text{ rad/s}$. Since the collision frequency is normally in the megahertz scale [16], which is several orders of magnitude lower than the frequency of the electromagnetic field of interest, it will be neglected in the subsequent investigation of EFCs of the magnetized plasma.

We first plot the critical parameters ε_R , ε_L , ε_p , and ε_X for the electromagnetic frequency below the plasma frequency at an applied magnetic field of 4 T, in Fig. 1(a). The presence of the magnetic field leads to different dispersions for left-handed (LH) and right-handed (RH) circularly polarized electromagnetic waves propagating along the magnetic field, with refractive indices $\sqrt{\varepsilon_{L(R)}}$, which could be real even for the electromagnetic frequencies below the plasma frequency. The two modes become elliptically polarized for $0 < \theta < \pi/2$. At $\theta = \pi/2$, the LH and RH modes turn into ordinary and extraordinary modes, with polarization parallel and perpendicular to the applied magnetic field, and refractive indices given by $\sqrt{\varepsilon_p}$ and $\sqrt{\varepsilon_X}$, respectively.

As shown by Fig. 1(a), for electromagnetic frequency below the plasma frequency, the LH mode exhibits a positive dielectric constant ($\varepsilon_L > 0$) for propagation along the applied magnetic field and a negative dielectric constant ($\varepsilon_p < 0$) for propagation perpendicular to it, indicating an unbounded EFC for the LH mode. This is confirmed by the plots of EFCs for an electromagnetic frequency of 1 GHz ($\lambda = 30 \text{ cm}$), or $\omega = 6.28 \times 10^9 \text{ rad/s}$ at several applied magnetic fields ranging from 1 to 4 T [Fig. 1(b)]. At large dc magnetic field ($> 3 \text{ T}$), there exist two EFCs, one bounded (RH) and the other extending to infinity (LH),

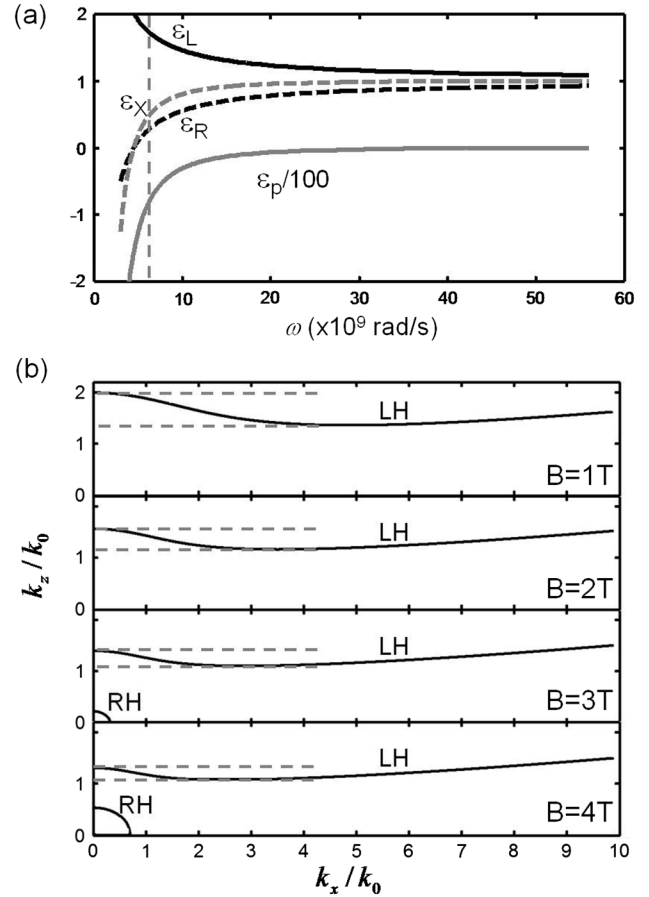


FIG. 1. (a) Four critical parameters determining the dispersion of magnetized plasma: ε_R , ε_L , ε_p , and ε_X vs electromagnetic frequency at an applied magnetic field of 4 T. The vertical dashed line shows the frequency at which the EFCs are plotted. (b) The EFCs of plasma under a magnetic field ranging from 1 to 4 T. The horizontal dashed lines in each figure indicate flatness of the EFC of the left-handed mode.

reminiscent of the EFCs of the transverse-electric-field (TE) and transverse-magnetic-field (TM) modes in a hyperbolic medium. For the magnetic field below a cutoff value (2.85 T), the permittivity of the RH mode becomes negative and its propagation is not supported in the plasma anymore. As a result, its EFC disappears at a lower magnetic field of 1 and 2 T in Fig. 1(b).

To investigate the strength of the magnetized plasma in imaging, we carried out numerical simulations on wave propagation with subdiffraction features by using commercial software—COMSOL. The configuration is shown in Fig. 2. The object to be imaged consists of three holes, positioned in a triangle, with a diameter of $\lambda/7.5$ and spacing of $\lambda/5$ in a perfect electric conductor (PEC) film, which is separated by $\lambda/30$ from the plasma. A plane electromagnetic wave of 1 GHz frequency is incident normal to the PEC film. The plasma frequency is kept the same as before ($\omega_p = 5.64 \times 10^{10} \text{ rad/s}$), whereas a very large collision frequency $\gamma = 5 \text{ GHz}$ is assumed (2 orders of magnitudes larger than that in Ref. [16]) to

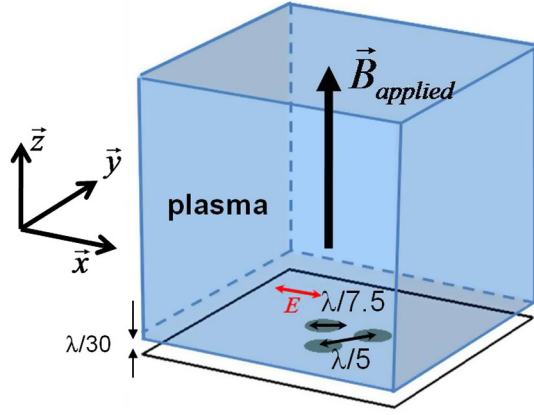


FIG. 2 (color online). Schematic of an imaging system based on the magnetized plasma. The object consists of three subwavelength circular apertures in a PEC film, with the detailed geometry shown in the figure. The magnetic field is along the z direction. A plane wave is incident upon the object at the normal direction from underneath the object, with the polarization indicated.

ensure the convergence of the simulation. The permittivity tensor taking into account the finite collision frequency is given by [17]

$$\varepsilon = 1 + \frac{i\omega_p^2}{\omega\gamma} \times \begin{pmatrix} \frac{1-i\omega/\gamma}{(1-i\omega/\gamma)^2 + \omega_c^2/\gamma^2} & \frac{-\omega_c/\gamma}{(1-i\omega/\gamma)^2 + \omega_c^2/\gamma^2} & 0 \\ \frac{\omega_c/\gamma}{(1-i\omega/\gamma)^2 + \omega_c^2/\gamma^2} & \frac{1-i\omega/\gamma}{(1-i\omega/\gamma)^2 + \omega_c^2/\gamma^2} & 0 \\ 0 & 0 & \frac{1}{1-i\omega/\gamma} \end{pmatrix}. \quad (4)$$

The distribution of the electric field is shown in Fig. 3. The fields plot in the x - z plane presents a direct view on how the wave propagates inside the plasma [Fig. 3(a)]. At the lowest magnetic field of 1 T, the waves emerging from the holes interfere and form a diffraction pattern after propagating through a certain distance. As a result, the pattern of the three holes is not transported to the image side, as shown in Figs. 3(b) and 3(c). However, it is worth noting that the subwavelength spatial information of the object is still contained in the diffraction pattern, as the waves with large in-plane wave vectors can propagate through the magnetized plasma. As the magnetic field increases, the electromagnetic waves start to exhibit almost diffractionless propagation and are confined in narrow beams with deep subwavelength width. This can be attributed to a flatter EFC at higher magnetic field (Fig. 1). A standing wave pattern is formed along the propagation due to the impedance mismatch at the plasma-air interface. Diffractionless propagation is very important for the imaging, as illustrated by Figs. 3(b) and 3(c), where three bright spots are clearly observed both inside and outside the plasma at higher magnetic fields of 3 and 4 T, corresponding to the images of the three apertures in the PEC film. However, the images right outside the plasma in Fig. 3(b) are somewhat distorted, whereas inside the plasma, the

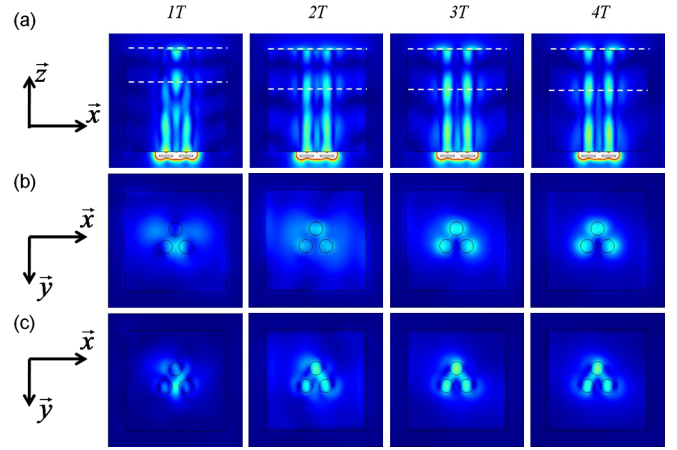


FIG. 3 (color online). The simulated field distribution at a magnetic field ranging from 1 to 4 T. In the calculation, a higher collision frequency is assumed to assure the convergence of the calculation. (a) Field plot in an x - z plane that intercepts the centers of two holes aligned along the x direction. (b) Field plot in an x - y plane right outside the plasma on the image side (output plane). (c) Field plot in an x - y plane inside the plasma at the antinode of the standing wave, as indicated by the white dashed lines in (a).

field plots faithfully exhibit the same pattern as the object [Fig. 3(c)]. The difference between the field plots inside and outside the plasma can be attributed to the large discontinuity of the z component of the electric field at the interface between the plasma and air. This is confirmed by the plot of the x and z components of the electric field at the 4 T magnetic field in Fig. 4. Inside the plasma, the total electric field is dominated by the x component; in comparison, the z component is almost negligible. Across the interface, the z component of the electric displacement field is continuous, and, due to the large permittivity of the plasma along the surface normal, the z component of

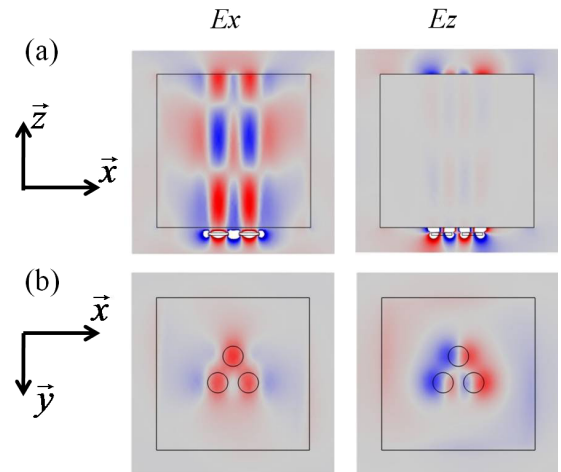


FIG. 4 (color online). The field plots of the x and z components of the electric field at the 4 T magnetic field in the (a) x - z plane and (b) x - y output plane.

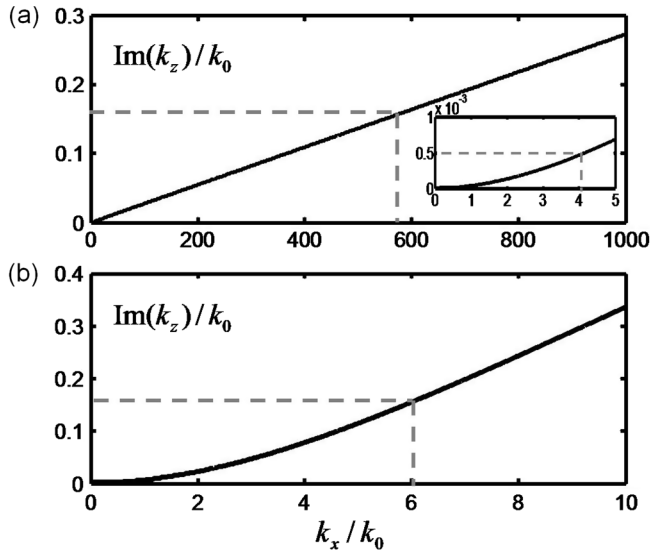


FIG. 5. (a) Plot of $\text{Im}(k_z)$ vs k_x for the same parameters as in Fig. 1, but with a realistic collision frequency of 30 MHz taken from Ref. [16]. The inset shows a zoom-in view of the plot for k_x up to $5k_0$. (b) The same as (a) but with an exaggerated collision frequency of 5 GHz.

the electric field outside the plasma is significantly larger than that inside the plasma and comparable to the magnitude of the x component. Therefore, one possible solution for imaging would be a polarization-selective detection wherein only the in-plane (x - y) component of the electric field is measured.

The imaging resolution of the magnetized plasma system is fundamentally limited by the material loss and thickness of the plasma. This is evident from the plot of $\text{Im}(k_z)$ vs k_x [Fig. 5(a)], obtained by combining Eq. (4) and the wave equation, for a plasma under a magnetic field of 4 T, and with a realistic colliding frequency of 30 MHz taken from Ref. [16]. The imaginary part of k_z increases linearly at large k_x , indicating that the waves containing information of higher spatial resolution experience higher propagating loss. The resolution is inversely proportional to the thickness of the magnetized plasma d , as the attenuation is characterized by $e^{-\text{Im}(k_z)d}$. Given a magnetized plasma with a thickness λ_0 as in the configuration shown in Fig. 2, the spatial resolution can be estimated by $\text{Im}(k_z)\lambda_0 = 1$, or $\text{Im}(k_z)/k_0 = 0.16$, which, according to Fig. 5(a), corresponds to an extremely large cutoff in-plane wave vector $k_x = 585k_0$, or an imaging resolution of $\lambda_0/1170 = 256 \mu\text{m}$. The inset in Fig. 5(a) shows $\text{Im}(k_z)/k_0 = 5 \times 10^{-4}$ for $k_x = 4k_0$, which means that the feature size of $\lambda_0/8$ can be transported through a plasma of $320\lambda_0$ thick. As shown by Fig. 5(b), even with an exaggerated collision frequency of 5 GHz, the cutoff in-plane wave vector for imaging after a propagation length of λ_0 is given as $k_x = 6k_0$, corresponding to an imaging

resolution of $\lambda_0/12$. This is consistent with the simulation results shown in Figs. 3 and 4, where features as small as $\lambda_0/7.5$ can be resolved.

The imaging system based on magnetized plasma can be readily modified to curved configurations, with a magnetic field approximately along the radial directions, to form a hyperlens [11]. Imaging with magnetized plasma can be extended to radio frequencies where important applications such as magnetic resonance imaging may benefit from the capability of transportation and magnification of deep subwavelength features. In certain doped semiconductors such as indium antimonide (InSb), the effective mass of electrons is almost 2 orders of magnitude less than its free space mass; therefore, the cyclotron frequency can easily reach terahertz with a readily available magnetic field. Thus, reconfigurable subdiffraction imaging using magnetized plasma may bring important applications to the terahertz as well.

The simulation in this work was supported by the U.S. DOE (DE-AC02-05CH11231), and the rest was supported by the NSF Nano-scale Science and Engineering Center (CMMI-0751621).

*Present address: School of Physics and Astronomy, University of Birmingham, Birmingham, B15 2TT, United Kingdom.

†To whom all correspondence should be addressed. xiang@berkeley.edu

- [1] V.G. Veselago, *Sov. Phys. Usp.* **10**, 509 (1968).
- [2] J.B. Pendry, *Phys. Rev. Lett.* **85**, 3966 (2000).
- [3] N. Fang, H. Lee, C. Sun, and X. Zhang, *Science* **308**, 534 (2005).
- [4] T. Taubner *et al.*, *Science* **313**, 1595 (2006).
- [5] J.B. Pendry, D. Schurig, and D.R. Smith, *Science* **312**, 1780 (2006).
- [6] D. Schurig *et al.*, *Science* **314**, 977 (2006).
- [7] A. Grbic and G.V. Eleftheriades, *Phys. Rev. Lett.* **92**, 117403 (2004).
- [8] D.R. Smith and D. Schurig, *Phys. Rev. Lett.* **90**, 077405 (2003).
- [9] Zubin Jacob *et al.*, *Opt. Express* **14**, 8247 (2006).
- [10] A. Salandrino and N. Engheta, *Phys. Rev. B* **74**, 075103 (2006).
- [11] Z.W. Liu *et al.*, *Science* **315**, 1686 (2007).
- [12] J. Yao *et al.*, *Science* **321**, 930 (2008).
- [13] P.A. Belov *et al.*, *Phys. Rev. B* **77**, 193108 (2008).
- [14] M. Wiltshire *et al.*, *Science* **291**, 849 (2001).
- [15] P.W. Bellan, *Fundamental of Plasma Physics* (Cambridge University Press, Cambridge, England, 2006).
- [16] Y.P. Bliokh, J. Felsteiner, and Y.Z. Slutsker, *Phys. Rev. Lett.* **95**, 165003 (2005).
- [17] Y.M. Strel'niker and David J. Bergman, *Phys. Rev. B* **77**, 205113 (2008).